Title
Neutrino Physics from the Cosmic Microwave Background and Large-Scale Structure

Journal
Annual Review of Nuclear and Particle Science, 66(1)

ISSN
0066-4243

Authors
Abazajian, Kevork N
Kaplinghat, Manoj

Publication Date
2014-10-01

DOI
10.1146/annurev-nucl-102014-021908

Peer reviewed

Neutrino Physics from the Cosmic Microwave Background and Large-Scale Structure

Kevork N. Abazajian and Manoj Kaplinghat

Center for Cosmology, Department of Physics and Astronomy, University of California, Irvine, California 92697; email: kevork@uci.edu, mkapling@uci.edu

Annu. Rev. Nucl. Part. Sci. 2016. 66:401–20

First published online as a Review in Advance on July 14, 2016

The *Annual Review of Nuclear and Particle Science* is online at nucl.annualreviews.org

This article's doi:
10.1146/annurev-nucl-102014-021908

Keywords

neutrinos, cosmology, large-scale structure, cosmic microwave background

Abstract

Cosmology and neutrino physics have converged into a recent discovery era. The success of the standard model of cosmology in explaining the cosmic microwave background and cosmological large-scale structure data allows for the possibility of measuring the absolute neutrino mass and providing exquisite constraints on the number of light degrees of freedom, including neutrinos. This sensitivity to neutrino physics requires the validity of some of the assumptions, including general relativity, inflationary cosmology, and standard thermal history, many of which can be tested with cosmological data. This sensitivity is also predicated on the robust handling of systematic uncertainties associated with different cosmological observables. We review several past, current, and future measurements of the cosmic microwave background and cosmological large-scale structure that allow us to do fundamental neutrino physics with cosmology.

Contents

1. INTRODUCTION

Neutrinos are the most elusive known particles in nuclear and particle physics experiments. Remarkably, because the neutrinos are second only to photons in number density in the Universe, the study of cosmology via the largest physical structures can reveal properties of the neutrinos. Given the now-well-established nonzero mass of neutrinos, their high number density leads them to dominate, at present, the energy density of the cosmic microwave background (CMB) of photons by at least 25 times. The high density of neutrinos causes them to have significant effects on the growth of large-scale structure, even if they have small masses. A number of cosmological observables are sensitive to the presence of neutrinos through their effect on the expansion history and the growth of perturbations.

The possibility that cosmology could make robust measurements of particle constituents of the Universe such as neutrinos arose from a scientific revolution in physical cosmology in the late twentieth century—specifically, the emergence of concordance cosmology, now referred to as the standard model of cosmology with cold dark matter and a cosmological constant (ΛCDM). This model became widely adopted with the discovery of accelerating expansion in Type Ia supernova observations, which indicated a nonzero vacuum energy such as a cosmological constant, Λ (1, 2). These observations were almost concurrent with early CMB anisotropy measurements that indicated a flat geometry of the Universe. A nonzero Λ was then concordant with the low cosmological matter density being inferred from large-scale structure data. Observational results fell in line with the theoretical preference for a Universe with no curvature ($\Omega_{\rm tot} = \Omega_\Lambda + \Omega_b + \Omega_m = 1$), which avoids the flatness problem and is predicted by inflationary cosmology (see, e.g., Reference 3).

Around the same time, the zenith-angle dependence of the atmospheric neutrino flux was precisely measured, providing strong evidence for neutrino oscillations, consistent with neutrino mass splittings of $|\delta m^2_{\rm atm}|^{1/2} \approx 50$ meV between the states most closely associated with muon and tau flavor neutrinos (4). Along with this, the evidence of solar neutrino oscillations (5, 6) indicated that there is an additional splitting of $|\delta m^2_{\odot}|^{1/2} \approx 9$ meV. The two mass splittings are easily accommodated in three-flavor models that mirror the flavor structure of the charged leptons and quarks. However, there exist anomalies in short-baseline neutrino experiments, first observed in the Liquid Scintillator Neutrino Detector (LSND) experiment (7) and then in the MiniBooNE experiment (8), that could be the result of neutrino oscillations with a mass splitting of $|\delta m^2_{\rm SBL}|^{1/2} \sim 1$ eV. There is also a potential discrepancy in reactor neutrino experiments that could indicate a high mass splitting (9, 10). This third mass splitting would then require, at minimum, a fourth mass eigenstate in the neutrino sector, with the Z_0 width requiring the state to be sterile (11).

With the concurrent rise of precision cosmology and precision neutrino oscillation experiments, a massive cosmic neutrino background was predicted to have a measurable effect on proposed observations of cosmological large-scale structure; this prediction was made in a seminal paper on the luminous red galaxy (LRG) sample of the then-proposed Sloan Digital Sky Survey (SDSS) of galaxies (12). In Section 2, we discuss the physical mechanisms that make cosmological observables sensitive to the neutrino mass and then review the expected constraints.

The splittings of the mass eigenstates are becoming more precisely measured in oscillation experiments (13). The value of the absolute mass is more challenging to measure because it requires accurate measurement of the endpoint of the spectrum of β-decay neutrinos (14). Neutrinoless double-β decay experiments are also sensitive to absolute mass and will be able to determine whether neutrinos are Majorana particles (i.e., their own antiparticles) (15). Long-baseline neutrino oscillation experiments will also be able to determine whether the mass eigenstates of neutrinos have normal order, with $m_1 < m_2 < m_3$, or inverted order, with $m_3 < m_1 < m_2$; moreover, the absolute mass could reveal the nature of their mass-generation mechanism and provide a window into high-energy-scale physics (16).

The total mass of the neutrino mass eigenstates, $\Sigma m_\nu = m_1 + m_2 + m_3$, determines their effect on cosmology to a good approximation, although an exact treatment would include each neutrino mass uniquely. Solar and atmospheric oscillation results indicate that the sum is, at minimum, $\Sigma m_{\nu,\rm min} = |\delta m^2_{\odot}|^{1/2} + |\delta m^2_{\rm atm}|^{1/2} \approx 60$ meV. Minimal cosmological models with massive neutrinos are predicted to be sensitive to the atmospheric mass splitting. However, reaching this sensitivity requires that the systematics in these observations be subdominant to the effects of massive neutrinos, especially when combining different data sets. Already, tension exists between certain sets of cosmological observations, leading to an inferred total neutrino mass of $\Sigma m_\nu \approx 300$ meV. This may be evidence of a degenerate mass spectrum of the neutrinos ($m_1 \approx m_2 \approx m_3$), or the existence of a fourth mass eigenstate that is potentially consistent with short-baseline experiments. Both the high-sensitivity data and the signals of tension demonstrate the model dependence of the cosmological inferences of neutrino masses. The tension data could also indicate new cosmological physics, or they could be the result of unknown systematic errors in the data sets. We review these possibilities as well.

2. COSMOLOGICAL NEUTRINOS AND LARGE-SCALE STRUCTURE

2.1. Brief Thermal History of Neutrinos

The CMB is a thermal black body that requires a hot, dense early phase in the Universe. The current photon temperature is $T_{\gamma,0} = 2.72548 \pm 0.00057$ K (17), and the current photon density is $n_{\gamma,0} = 410.7\,(T_{\gamma,0}/2.72548\text{ K})^3$. At early times, the photon background had higher temperatures that increased inversely with the scale factor $T \propto a^{-1}$, as long as the number of degrees of freedom coupled to the photons was constant. The photon number density also increased at earlier times as $n_\gamma \propto a^{-3}$. At $T_\gamma \gtrsim 1$ MeV, photons are thermally coupled to a thermal neutrino background via the standard model interactions $\gamma + \gamma \leftrightarrow e^+ + e^- \leftrightarrow \nu_\alpha + \bar{\nu}_\alpha$. The cross sections for the weak processes $\nu e \leftrightarrow \nu e$ and $e^+e^- \rightarrow \nu\bar{\nu}$ are given by $\sigma \approx G_{\rm F} T^2$, where $G_{\rm F}$ is the Fermi constant, and the number density of the completely thermal neutrinos is

$$n_\nu = \frac{3\zeta(3)}{4\pi^2} g T_\nu^3. \qquad 1.$$

Here, g is the number of spin states of the neutrinos, and ζ is the zeta function. The interaction rate per neutrino is therefore $\Gamma_\nu = n\sigma|v| \sim G_{\rm F}^2 T_\nu^5$.

It is common to denote the effective number of neutrinos relative to a single neutrino density as in Equation 1:

$$N_{\rm eff} \equiv \frac{\rho_{\rm rel} - \rho_\gamma}{\rho_\nu}. \qquad 2.$$

The effective number, similar to a specific density, parameterizes the total radiation density ρ_r in units of a single thermal neutrino density: $\rho_\nu = 3.15 n_\nu T_\nu$.

If the neutrinos instantaneously decoupled from the photon background and electron–positron plasma, they would become cooler than the photons when the temperature of the Universe drops below the mass of the electron and electron–positron pairs annihilate, transferring their entropy to the photon background (18). The temperature of the neutrinos relative to the photons would then become

$$\frac{T_\gamma}{T_\nu} = \left(\frac{11}{4}\right)^{1/3} \approx 1.40. \qquad 3.$$

However, the decoupling of the neutrinos from the plasma is not instantaneous, and a small amount of the entropy from electron–positron pairs is transferred to the neutrinos.

The small amount of entropy from electron–positron pairs increases the number density of relativistic neutrinos, and distorts the energy distribution of the neutrinos away from a thermal spectrum. The effective relativistic energy in the standard neutrinos has been calculated as $N_{\rm eff} =$ 3.04–3.052 (19–21). The exact effects of the neutrino heating are, of course, not parameterized fully by $N_{\rm eff}$ but are more accurately described by their energy or momentum space distribution functions or, even more accurately, by the full momentum-dependent quantum density matrix of the neutrino species. Because the heating of neutrinos is of order 1%, the effect is typically included as an increase in the pure relativistic energy density.

At later times, massive neutrinos become nonrelativistic when $T_\nu \lesssim m_\nu$ and cluster as hot dark matter. The late-time contribution of massive neutrinos to the cosmological matter density as a fraction of the critical density, $\Omega_\nu = \rho_\nu/\rho_{\rm crit}$, is

$$\Omega_\nu = \frac{\Sigma m_\nu n_\nu}{\rho_{\rm crit}} \approx \frac{\Sigma m_\nu}{94.10 \text{ eV } h^2}, \qquad 4.$$

where Σm_ν is the sum of the three standard neutrino mass eigenstates and the Hubble constant is parameterized as $h \equiv H_0/(100 \text{ km s}^{-1} \text{ Mpc}^{-1})$. The numerical value on the right-hand side is calculated for $N_{\rm eff} = N_\nu = 3$, but is clearly altered for heated standard neutrinos or nonstandard effects. The contribution of neutrinos to the critical density as matter-like particles changes the contribution of other matter, the evolution of cosmological inhomogeneities, the growth of structure, and the properties of anisotropies in the CMB. We review these effects below, along with the observational constraints on the standard cosmological neutrinos.

The neutrinos could be nonthermal, and $N_{\rm eff}$ could differ drastically from the standard value of approximately 3.05 if there were a nonstandard thermal history (22, 23), if there are new light sterile neutrinos that mix with active neutrinos (24), or if neutrinos have nonstandard interactions (25). Many constraints on these scenarios have been explored. We review these cases below.

2.2. Neutrinos and the Evolution of Cosmological Inhomogeneities

Here, we discuss the physical effects of the standard massive neutrinos on the distribution and clustering of large-scale structure. These effects are of two types. First, at early times, massive neutrinos could alter the decay of the gravitational potential in the radiation-dominated early Universe. Second, the neutrinos free-stream at late times to suppress the growth of structure in the linear regime. Although related, and sometimes conflated, these are distinct effects.

The evolution of inhomogeneities in the early Universe is linear, which simplifies calculations. The gravitational potential, Φ, that governs the linear growth of structure is set by the primordial potential. This potential is then modified by early-epoch evolution, quantified by the transfer function, and further changed by the growth function at late times (26):

$$\Phi(k,a) = \Phi_{\rm p}(k) \times \{\text{transfer function}(k)\} \times \{\text{growth function}(k,a)\}, \qquad 5.$$

where k is the wave number of the potential. The power spectrum of the primordial potential $\Phi_{\rm P}$ is assumed to be of the form motivated by inflation, $P_\Phi(k) \propto k^{-4}\, k^n$, where n is the primordial scalar perturbation index. The evolution of the gravitational potential during the matter-dominated era with massless neutrinos is simple: It stays roughly constant for all values of k. In our Universe, with massive neutrinos, the growth function is dependent on wave number as well as scale factor (27).

Because neutrinos are known to be light, their behavior was modified from radiation-like when $T_\nu \gg m_\nu$ to matter-like when $T_\nu \ll m_\nu$ between matter–radiation equality and today. To demonstrate the effects of massive neutrinos without varying other parameters, we fix the total matter density and the primordial power spectrum. The matter density is specified as $\Omega_m = \Omega_\nu + \Omega_{\rm DM} + \Omega_b$, where $\Omega_{\rm DM}$ and Ω_b are the fractions of the critical density in dark matter and baryons, respectively.

Neutrinos cannot cluster on length scales smaller than their free-streaming scale, which in turn affects dark matter perturbations. So, on scales smaller than the neutrino free-streaming scale, there will be a suppression of the matter power spectrum. In detail, the scale-dependent suppression is controlled by the competition between the temperature (velocity dispersion) of the neutrino and the gravity of the clustering matter component (dark matter), determined by a comparison of the relevant modes to the Jeans length.

The wave number corresponding to the free-streaming scale of neutrinos is typically defined in analogy to the Jeans length. The key point for our discussion is that the free-streaming length scale is proportional to $m_\nu^{-1/2}$. For our purposes, a reasonable approximation to the free-streaming wave number is

$$k_{\rm fs} = \frac{[4\pi G \rho_M(z_{\rm nr})]^{1/2}}{v_\nu(1+z_{\rm nr})}, \qquad 6.$$

$$\approx 0.02 \left(\frac{\Omega_m h^2 m_\nu}{\rm eV}\right)^{1/2} {\rm Mpc}^{-1}, \qquad 7.$$

where $\rho_M \propto (1+z)^3$ is the density of all the matter that clusters; $v_\nu = 3.15 T_\nu / m_\nu$ is the mean thermal speed of the neutrinos; and Equations 6 and 7 have been calculated at the epoch when $3.15 T_\nu = m_\nu$, which is an estimate of when neutrinos become nonrelativistic. The factor of $1+z$

in the denominator of Equation 6 is there to make k_{fs}^{-1} a comoving length scale, namely the scale length as measured today. Once the neutrinos become nonrelativistic, their velocity decays inversely with the scale factor: $v_\nu = 151(m_\nu/\text{eV})^{-1}(1+z)$ km s^{-1}. Thereafter, the comoving free-streaming length scale k_{fs}^{-1} actually decreases with expansion. This is the reason for choosing the time when neutrinos become nonrelativistic as the epoch to compute the comoving free-streaming wave number, whose effects are imprinted in the matter power spectrum. The free-streaming scale shows that the suppression shifts to smaller scales (larger wave numbers) as the neutrino mass increases. Note that the suppression scale is determined by the individual neutrino masses, so in principle large-scale structure data are directly sensitive to the mass ordering and not simply the sum of the masses, but it does not seem possible to tease out this information.

Another way to interpret the above scale is through the mode that enters the horizon when neutrinos become nonrelativistic, $k_{nr} = H(z_{nr})/(1+z_{nr})$, which is closely related to k_{fs}. Modes that come into the horizon before this epoch, that is, when $k > k_{nr}$, will show suppression compared with the fiducial model because we have essentially replaced some cold dark matter with a neutrino component that is not nonrelativistic.

The amplitude of the suppression is related to the energy density in neutrinos. An estimate of the magnitude of this suppression on the small scales is

$$\frac{\Delta P_\delta}{P_\delta} \approx -8\frac{\Omega_\nu}{\Omega_m} = -8\frac{\Sigma m_\nu}{94\ \Omega_m h^2\ \text{eV}}, \qquad 8.$$

where we have given the neutrinos mass and kept the relativistic energy density and matter density fixed. The power spectrum $P_\delta(k)$ of the total matter density fluctuations δ is defined as $\langle\delta(\vec{k})\delta(\vec{k}')\rangle = P_\delta(k)\delta^3(\vec{k}-\vec{k}')$. Note that the suppression is proportional to the fraction of the energy density of matter that is in neutrinos: $f_\nu = \Omega_\nu/\Omega_m$. If we keep f_ν fixed and increase the neutrino mass, which implies a nonthermal abundance of the neutrinos, then the suppression decreases over the observable range of scales because the free-streaming scale shifts to smaller physical scales.

The factor of eight in Equation 8 arises from the energy density contributed by the nonclustering neutrinos (which would give rise to $\Delta P_\delta/P_\delta \approx -2f_\nu$) and the feedback of the presence of nonclustering neutrinos on the density fluctuations of the rest of the matter. This feedback results from the fact that on scales $k \gg k_{fs}$, where neutrinos are not able to cluster, the general relativity equation for the gravitational potential Φ reads $2k^2(1+z)^2\Phi = +3H^2(1-f_\nu)\delta_{cold}$, where δ_{cold} stands for the fluctuations in the component that is able to cluster (dark matter other than neutrinos). Note that $H^2(1-f_\nu) \propto \rho_M - \rho_\nu$. The gravitational potential Φ provides the source term for the growth of δ (26), and the presence of the $1-f_\nu$ term in the Poisson equation slows down the growth of perturbations. Instead of the growth increasing with the scale factor $\delta_{cold} \propto a \propto 1/(1+z)$, we obtain $\delta_{cold} \propto (1+z)^{3f_\nu/5-1}$ (27, 29); thus, the resulting fractional difference $\Delta P_\delta/P_\delta$ increases with time. The final suppression works out to $-8f_\nu$ (12, 28). The full numerical effects of massive neutrinos on the power spectrum are depicted in **Figure 1**, which shows the suppression described above. For large enough k, all modes see similar suppression upon crossing the horizon and, hence, the relative difference in plateaus. Note that if the comparison were done in a way in which the total matter density was not kept fixed, then the maximal change would be less than $-8f_\nu$.

Although the detailed shape of the suppression due to massive neutrinos is hard to mimic, there will be some model dependence in inferring neutrino properties with data over a limited range of k. First, the effect of massive neutrinos on the transfer and growth functions (Equation 5) can be degenerate with the primordial power spectrum. Second, the effect on the growth function can be degenerate with the modifications introduced to the late-time expansion history by evolving

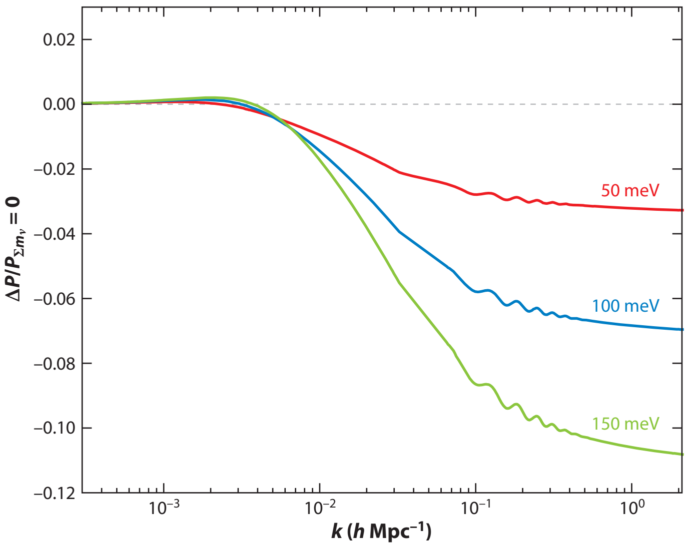

Figure 1

The changes to the matter power spectrum at the present time due to the addition of masses for neutrinos. The total matter density today, which includes massive neutrinos and dark matter, is kept fixed by lowering the dark matter density appropriately. The scale-dependent suppression occurs because massive neutrinos do not cluster like cold dark matter on small scales.

dark energy (30). This is because the growth function is governed by differential equations whose solution depends on the expansion history.

2.2.1. Nonstandard neutrinos and their effects. As described in Section 1, there are many anomalies that could be indicative of neutrino oscillations over short baselines in reactor and beam experiments. These oscillations would require a new mass eigenstate associated with a neutrino with no weak interactions: a sterile neutrino. Sterile neutrinos with mixings consistent with the short-baseline LSND experiment would be thermalized in the early Universe and contribute to extra relativistic degrees of freedom at early times, as well as to Σm_ν.

The precise effect of an extra sterile neutrino depends on the nature of the mass hierarchy motivated by the short-baseline result. For some cases, a sterile neutrino is thermalized, affecting structure formation via contributions to both the early relativistic energy density and the late massive neutrino density. For other cases, the sterile neutrino resonantly generates lepton number through a Mikheyev–Smirnov–Wolfenstein-type mechanism that can suppress thermalization (31). However, in the full four-neutrino framework, the sterile neutrino can lead to multiple resonant-level crossings, which make the neutrino densities and spectra unpredictable, given current neutrino parameter uncertainties (32). The prospect of a full or partially thermalized sterile neutrino is interesting because there exists tension in subsets of cosmological data that could be due to massive neutrinos and/or extra relativistic degrees of freedom, which we discuss below.

New nonstandard neutrino interactions, such as a new self-interaction (33), neutrino decay (34), or late neutrino mass generation (35, 36), would also alter the effects of neutrinos from early to late times. Such cases are strongly constrained by a combination of the CMB and large-scale structure data (37, 38). In particular, the acoustic phase shift due to free-streaming relativistic radiation (39) has been detected in high–angular resolution CMB observations (40), and it offers a model-independent way to constrain the free-streaming component of $N_{\rm eff}$ (41). The relativistic energy density (not including photons) also has a sound speed consistent with the thermal neutrino background. While these new physics ideas illustrate the model dependence inherent in any cosmological analysis aiming to measure a particle property, it is encouraging that multiple cosmological observables could be used to break degeneracies.

2.3. Small-Scale Structure

At late times, where the growth of inhomogeneities enters the nonlinear self-gravitating regime, massive neutrinos will participate in the nonlinear clustering (42, 43). Although the enhancement of density in a Milky Way–type dark matter halo is, at most, a factor of several, it has significant implications for direct detection of the relic neutrino background in terrestrial experiments (44). In addition, the nonlinear neutrino clustering has been extensively simulated (45), and although the effect is small, it may affect the inferred cosmology from clustering of dark matter and gas in observational probes such as weak lensing and the Lyman-α forest (46–48).

3. LARGE-SCALE STRUCTURE OBSERVABLES

The diverse, independent, and often complementary methods available in cosmological surveys to measure the same physical effect will play a crucial role in making a robust measurement of the sum of neutrino masses, nonstandard interactions of neutrinos, the number of sterile neutrinos, or the deviation of $N_{\rm eff}$ from three. In the subsections below, we describe some of the methods currently in use and the prospects for measuring neutrino properties from future planned surveys.

3.1. Galaxy Redshift Surveys

The initial prediction that the emerging standard cosmological model could constrain neutrino masses was made with galaxy redshift surveys, specifically the LRG sample of the SDSS, a three-dimensional survey of galaxies using spectroscopically determined distances (12). The Fourier transform of the correlation function of galaxies, their power spectrum $P_g(k)$, is a scale-independent biased tracer of the linear matter power spectrum $P_m(k)$ on large scales. In other words, $P_g(k, z) = b^2 P_m(k, z)$, where b is the scale-independent bias parameter on sufficiently large scales and z is the effective redshift of the survey (49). The measurement of $P_g(k)$ then provides a measure of the primordial power plus its evolution to the epoch of the survey z. Marginalizing over b allows one to measure the influence of massive neutrinos on the shape of the matter power spectrum (**Figure 1**).

Initial galaxy redshift survey constraints on neutrino mass came from both the 2° Field Galaxy Redshift Survey (50) and the main galaxy sample of the SDSS (51). When the first stage of the SDSS was completed, there were 110,576 LRGs producing cosmological parameter constraints consistent with expectations (52, 53). Early forecasts estimated that the Planck mission observations of the temperature and polarization of the CMB, in combination with the SDSS LRG sample, would have 1σ errors of $\sigma(\Sigma m_\nu) = 210$ meV (54). These early expectations have been borne out by current results showing that $\Sigma m_\nu < 380$ meV at 95% CL for Planck plus SDSS based on the standard cosmology (55).

Future and ongoing galaxy surveys will use both photometrically and spectroscopically determined redshifts of large samples of galaxies. The errors on the galaxy power spectrum measured from a survey typically scale as

$$\Delta P_g(k) = \sqrt{\frac{1}{2\pi w(k)\Delta \ln k}}\left[P_g(k) + \frac{1}{n_g}\right] \qquad 9.$$

$$\propto V_{\text{eff}}^{-1/2}, \qquad 10.$$

where $w(k) = (k/2\pi)^3 V_{\text{eff}}$. V_{eff} is the effective volume of the survey, n_g is the galaxy number density, and $\Delta \ln k$ is the bin size at k in $\ln k$-space. Future surveys, discussed below, will survey fainter galaxies as well as increase n_g and, crucially, the effective survey volume. Ongoing surveys also employ multiple, often complementary ways of measuring the evolution of the matter power spectrum and the expansion history of the Universe. Specifically, they can simultaneously use expansion-history measures such as the baryon acoustic oscillation (BAO) feature, the weak lensing of galaxies, the abundance of clusters of galaxies, and the clustering of gas in the Lyman-α forest along the line of sight to distant quasars. We discuss these methods in the following sections.

3.2. Lensing of Galaxies

Deep imaging of the sky performed commensurately with galaxy and supernova surveys can measure a weak gravitational lensing distortion of the shapes of galaxies due to intervening large-scale structure (for a review, see Reference 56). Initial studies found the autocorrelation of the lensing shear signal to be a potential sensitive probe of neutrino mass, although it was prone to large uncertainties due to nonlinear clustering (57). Use of the linear information alone showed that tomographic weak lensing of galaxies, employing photometric redshift determinations, could simultaneously sensitively constrain neutrino masses and dark energy without the large uncertainties due to the nonlinear information (30). The information to constrain Σm_ν comes from a combination of geometric information in the lensing kernel and the matter power spectrum (30). There are significant observational challenges in turning the forecasts using weak lensing shear observations into reality, chief among them being a proper understanding of the point spread function, which is key to measuring the shapes of faint galaxies. Sufficiently precise calibrations of these uncertainties seem to be possible (58). Initial estimates of the results from weak lensing observations are in tension with combined CMB and BAO data, which we discuss below.

3.3. Baryon Acoustic Oscillation and Distance Scales

The evolution of the Universe from a radiation-dominated era when baryons and photons were coupled through scattering processes imprints a simple geometrical feature, termed BAO, at a specific scale in cosmological inhomogeneities. Following the advent of large-scale galaxy redshift surveys such as the SDSS, BAO was quickly found to be a highly sensitive probe of the expansion history of the Universe (for a review, see Reference 59). BAO evolves with redshift with a dependence on the expansion history, which is affected by both dark energy and neutrino mass. The cosmological survey of SDSS was extended to the Baryon Oscillation Spectroscopic Survey (BOSS) of a larger volume of LRG galaxies, reducing errors accordingly (60).

The BAO feature is at large enough scales to be sufficiently robust to systematic effects such as nonlinear growth of structure and redshift space distortions (61). Because of the robustness of BAO to nonlinear effects, along with its strength as a cosmological constraint, CMB experiments have adopted it as a complementary external data set. Analyses using Planck 2015 and external data (62) used BAO data from the SDSS (63), BOSS LRG (64), and 6° Field Galaxy Survey (65).

The stringent Planck 2015 neutrino mass limit of $\Sigma m_\nu < 230$ meV(95% CL) resulted from a combination of BAO with the primary CMB temperature anisotropies, lensing of the CMB, supernova redshift distance measurements, and local Hubble constant measurements. This result excludes the Planck polarization spectra, which may be affected by low-level systematics but could provide stronger constraints on the total neutrino mass.

3.4. Lyman-α Forest

Distant bright quasars have broadband IR to UV emission that can provide a so-called backlight to intervening neutral gas. The absorption by gas along the line of sight produces a "forest" of absorption lines in quasar spectra blueward of the Lyman-α emission from the quasar itself. The intervening gas traces the large-scale structure of the Universe; its one-dimensional clustering can be a measure of the primordial matter power spectrum (66, 67), and its shape and amplitude could constrain neutrino mass (68). In initial modeling of the Lyman-α forest, the flux power spectrum in one dimension was linearly biased relative to the one-dimensional matter power spectrum. This implementation of a bias factor is similar to the implementation of constant galaxy bias discussed in Section 3.1, above. In fact, the biasing was found to be nonlinear, as well as dependent on cosmology and the thermal history of the gas. This dependence required numerical hydrodynamic simulations to relate the flux power to matter power, as well as a more sophisticated mapping between the gas and matter power spectrum in cosmological analyses (69).

The sensitivity of the Lyman-α forest lies in its dependence on the clustering of dark matter on very small scales, where massive neutrinos would suppress the matter power spectrum. This small-scale measurement provides information about neutrinos only in combination with precise measurements of the large-scale matter-clustering amplitude from the CMB.

There are theoretical modeling and observational challenges in the Lyman-α forest analyses. Importantly, the temperature history of the intergalactic medium (IGM) via the temperature density relation must be modeled at the same time as the primordial power spectrum evolution into the mildly nonlinear regime. This is generally done through simple parameterizations of the temperature density relation; however, the true temperature-density of the IGM and its evolution could be very different (70, 71).

3.5. Galaxy Clusters

Cosmological inhomogeneities that were initially linear have collapsed to structures on small scales, and the abundance of the structures provides an indirect measure of the amplitude and shape of the matter power spectrum at relatively small cosmological scales below ~10 Mpc or $k \approx 0.1h$ Mpc^{-1}. The abundance of the most massive gravitationally collapsed objects, clusters of galaxies with masses of 10^{14} to 10^{15} $M_\odot$, is highly sensitive to the amplitude of fluctuations on small scales, making them a potentially powerful probe of neutrino mass (72). The amplitude of the matter power spectrum at small scales is often parameterized by σ_8, the root-mean-square amplitude of fluctuations integrated over a scale of $8h^{-1}$ Mpc.

Clusters are detected in various wavelengths, from radio to γ-ray. The challenge in applying cluster surveys involves connecting the observable quantity, such as the number of optically detected galaxies, the X-ray flux, the weak lensing shear, or the Sunyaev–Zel'dovich (SZ) decrement, to the mass of the halo in which the cluster resides. The abundance of the mass of a given halo is what can be predicted, via numerical simulations, from the linear matter power spectrum. When combining the large-scale power spectrum determined from Planck, the number counts and the power spectrum probes from SZ radio surveys, such as the South Pole Telescope, and optical surveys, such as the Large Synoptic Survey Telescope (LSST), one may achieve a precision of $\sigma(\Sigma m_\nu) = 40$–$70$ meV (72). Historically, cluster abundance measurements of the amplitude of fluctuations were plagued by systematic uncertainties, yielding a range of values of the small-scale amplitude σ_8 (73, 74). Efforts are under way to cross-calibrate mass estimates by using weak lensing, SZ, X-ray, and galaxy number determinations, which could reduce systematic uncertainties in the mass–observable relations (see, e.g., Reference 75).

3.6. 21-cm Radio Surveys

Planned radio telescopes will map the 21-cm transition in hydrogen emitted as a function of redshift to enormous cosmological volumes. These observations will probe two main eras: the epoch of reionization at $6 \leq z \leq 12$, where a significant amount of neutral hydrogen is present, and the reionized Universe at $z \simeq 4$, where dense clumps of gas are targeted.

The 21-cm fluctuations of brightness temperature in the epoch of reionization arise from fluctuations in the ionized fraction of hydrogen, as well as from the primary fluctuations in the density (76). The epoch of reionization spans an enormous volume; therefore, incredibly small errors on the power spectrum can be obtained, in principle. In addition, at high redshifts such as $z \approx 8$, the nonlinear scale is $k_{\rm nl} \approx 2\ {\rm Mpc}^{-1}$, so information from much smaller scales can also be used. The number of wave-number modes captured increases commensurately.

Numerous instruments are already measuring the 21-cm sky. These include the Murchison Wide-field Array (MWA) (77), the Donald C. Backer Precision Array for Probing the Epoch of Reionization (PAPER) (78), the Giant Metrewave Radio Telescope (GMRT) (79), and the Low Frequency Array (LOFAR) (80). MWA's sensitivity to neutrino mass is predicted to be $\sigma(\Sigma m_\nu) \approx 100$ meV when combined with Planck priors (81). Future experiments with larger collecting areas and a greater number of baselines with an increase in antennae are being planned; examples are the Square Kilometer Array (SKA) and a proposed Fast Fourier Transform Telescope (FFTT) (76). There are important systematic effects that must be tamed in this pioneering method, including separation of foregrounds from the cosmological signal, potential scale-dependent galaxy bias and nonlinearity in the small-scale gas structure, and variations in the large-scale ionizing background. In the best-case scenarios, SKA is anticipated to get constraints of $\sigma(\Sigma m_\nu) = 20$ meV, whereas the FFTT could reach $\sigma(\Sigma m_\nu) = 3$ meV with Planck priors (82). These sensitivities degrade significantly when reionization modeling is required; for example, the error forecast for FFTT increases to $\sigma(\Sigma m_\nu) = 20$ meV (81).

3.7. Current and Future Galaxy and Quasar Surveys

In the subsections below, we describe some of the current and planned surveys that are targeting both galaxies and quasars and exemplifying the precision constraints one can expect from cosmology on the sum of neutrino masses. The primary science driver for these surveys is understanding the nature of dark energy.

3.7.1. eBOSS. The extended Baryon Oscillation Spectroscopic Survey (eBOSS) is a new redshift survey within SDSS-IV, which began making observations in July 2014 (83). eBOSS will extend the SDSS BAO measurement to $0.6 < z < 1$ by using LRGs and emission line galaxies (ELGs), and it will measure BAO at $0.9 < z < 2.2$ by using quasars. By combining information from eBOSS observations, including galaxy clustering, BAO, and the Lyman-α forest, forecasts indicate that $\sigma(\Sigma m_\nu) = 30$ meV should be possible, assuming single-parameter (Σm_ν) extensions to the standard cosmological model (84).

3.7.2. DES. The Dark Energy Survey (DES) uses a 520-MP camera on the 4-m Blanco telescope of the Cerro Tololo Inter-American Observatory (CTIO) to perform a 5,000-deg^2 multicolor imaging survey of the southern hemisphere. When combined with other imaging data, the data from DES will provide photometric redshifts for 180,000,000 galaxies out to $z = 1.5$, yielding a very large effective volume for galaxy power spectrum measures, as well as information about BAO and the weak lensing of galaxies (85). As a result, the outlook based on single-parameter (Σm_ν) extensions of the standard cosmological model is very good: $\sigma(\Sigma m_\nu) = 41$ meV (86).

3.7.3. DESI. The proposed Dark Energy Spectroscopic Instrument (DESI) will employ a 4-m Mayall telescope with a new spectrograph featuring 5,000 robotically actuated fibers covering a 3°-diameter field of view with a new optical corrector (87). DESI will increase the number of galaxies from SDSS-IV BOSS by an order of magnitude and will also increase the effective volume of the galaxy survey. Predictions for the DESI BAO sensitivity to neutrino mass range from $\sigma(\Sigma m_\nu) = 90$ meV with Planck data to $\sigma(\Sigma m_\nu) = 17$ meV from galaxy data plus Lyman-α forest clustering data (86).

3.7.4. LSST. The LSST is a wide-field, ground-based telescope that is designed to image a large fraction of the sky in six optical bands (88). It is anticipated to begin operation in 2019. The LSST will be capable of making photometric redshift galaxy clustering measurements and studying weak gravitational lensing, Type Ia supernovae, and galaxy cluster samples. Due to this powerful combination of cosmology probes, the LSST's predicted sensitivity to neutrino mass is $\sigma(\Sigma m_\nu) = 20$–$40$ meV with Planck priors (86, 89, 90).

3.7.5. Space missions: Euclid and WFIRST-AFTA. The European Space Agency's Euclid mission is a space mission comprising a 1.2-m mirror and optical and near-IR cameras that will perform weak lensing, photometric redshift galaxy clustering, and galaxy cluster surveys (91). It is planned to launch in 2020. The combination of cosmological probes make Euclid very sensitive to dark energy and neutrino masses. Forecasts using the shear autocorrelation of Euclid galaxies, as well as galaxy-shear cross-correlation, galaxy cluster abundances, and Planck priors, predict the best-case constraint $\sigma(\Sigma m_\nu) = 9.8$ meV (90). This sensitivity requires robust control over each of these observables' systematics.

The WFIRST-AFTA space mission will use a 2.4-m mirror with optical and near-IR cameras to perform BAO and Type Ia supernova surveys, as well as weak lensing and photometric redshift galaxy clustering surveys (92). It is planned to launch in the mid 2020s. Forecasts including Planck priors for WFIRST BAO with BOSS BAO data sets find $\sigma(\Sigma m_\nu) = 95$ meV; WFIRST photometric galaxy data plus BOSS galaxy clustering data should be much more constraining with $\sigma(\Sigma m_\nu) = 21$ meV (86).

3.8. Tension Among Data Sets

Many measurements of the amplitude of the matter power spectrum indicate that it is lower than that inferred from the Planck 2015 cosmology data with massless neutrinos (93–95). The tension among these data sets can be summarized using the amplitude of clustering of matter parameterized as σ_8. The value of σ_8 is inferred either indirectly from the cosmological parameters determined by the high-precision CMB measurements or more directly from the local measures of clustering or halo abundances. The value inferred from Planck temperature data and WMAP large angular scale ("low-ℓ") polarization data is $\sigma_8 = 0.829 \pm 0.014$ (62), whereas a combination of lensing and cluster data inferred a lower value with tight errors, $\sigma_8 = 0.7946 \pm 0.0094$ (94).

This tension could be resolved through the addition of neutrino mass and/or the addition of a new relativistic degree of freedom in $N_{\rm eff}$. Allowing for only massive standard active neutrinos yields $\Sigma m_\nu = 0.357 \pm 0.099$ eV, and a partially thermalized sterile neutrino is required to have a mass of $m_s = 0.450 \pm 0.124$ eV in the analysis in Reference 94. Results that are consistent with a different subset of cluster data find $\Sigma m_\nu = 0.357 \pm 0.099$ eV with an additional relativistic density of $\Delta N_{\rm eff} = 0.72 \pm 0.29$ in the pure standard active massive neutrino case, or $m_s = 0.48 \pm 0.14$ eV and an extra relativistic energy density $N_{\rm eff} = 0.61 \pm 0.31$ in the sterile neutrino case (93). Even the SZ cluster sample from Planck 2015 found weak evidence for nonzero neutrino mass (96). These results have been of interest because such a sterile neutrino could explain the anomalies in the short-baseline data. However, such a neutrino would be fully thermalized due to the relatively large mixing required for the short-baseline observations (97).

4. NEUTRINOS AND THE COSMIC MICROWAVE BACKGROUND

The CMB is a precision measure of the fluctuations in the energy density of the Universe at the time when the majority of the photons last scattered. The WMAP and Planck measurements of the temperature fluctuations in the sky today have provided a picture of this early structure that is beautifully consistent with the ΛCDM model with adiabatic initial conditions (62, 98). Several reviews discussing observations of the CMB and the physics that determines its features are available (see, e.g., Reference 99). Many of these features are changed when the masses and other properties of the neutrinos are varied, making the CMB a sensitive probe of neutrino physics (28).

4.1. Cosmic Microwave Background Anisotropies and Neutrino Mass

In the following discussion, we assume that the baseline model is ΛCDM with three massless neutrinos whose abundance is exactly as predicted by thermal history (described above). As above, we consider the main effects on the CMB of making the neutrinos massive, while keeping the total matter density (baryons, dark matter, and neutrinos) fixed. Doing so implies that the change in the angular diameter distance to the last scattering surface is small. However, the change in the energy budget at the last scattering surface, which arises from the fact that there is effectively one less relativistic neutrino, decreases the expansion rate during last scattering, $H_{\rm LSS}$. Because all length scales are proportional to $1/H_{\rm LSS}$, this leads to an increase in the sound horizon. The angle subtended by the sound horizon at last scattering has been exquisitely determined (to better than 0.1%), but the other cosmological parameters (matter density, dark energy parameters, and curvature) have a significantly larger effect on the sound horizon.

The change in the expansion rate also implies a change in the way that the gravitational potentials decay with time. The decay of these potentials drives the CMB anisotropy power because the photons fall in and out of these potential wells on their way to us from the last scattering surface. Again, however, this is not an avenue for a precision measurement of the neutrino masses, because of degeneracies with the matter density. The Planck temperature and polarization measurements can provide the constraint $\Sigma m_\nu < 0.49$ eV at 95% CL, assuming the standard ΛCDM parameters (62). Adding other data sets can help, as shown by an analysis using the 7-year WMAP data combined with H_0 measurements from the Hubble Space Telescope and SDSS-III Constant Mass (CMASS) sample of galaxies, which require $\Sigma m_\nu < 0.36$ eV at 95% CL (100). These constraints depend on the assumed model. For example, if dark energy is allowed to be a fluid with a constant equation of state (pressure over density), then the constraints worsen somewhat. An analysis of the clustering SDSS-III BOSS galaxies with Planck temperature data and 9-year WMAP polarization data found a constraint of $\Sigma m_\nu < 0.39$ eV at 95% CL for the

ΛCDM model, whereas the same analysis within the dynamical dark energy model (with a constant equation of state) obtained $\Sigma m_\nu < 0.49$ eV at 95% CL (101).

These results are exciting, but they are far from the 50-meV level. To approach this level, we need to add more data sets that can break the degeneracies between Σm_ν and other parameters, such as Ω_m and σ_8. When adding data sets, one must be careful with the systematics associated with different data sets, and ensure that the data sets are not in tension. A recent analysis using the SDSS-III BOSS Lyman-α data and Planck data, including a detailed assessment of known systematics, achieved a spectacular constraint of $\Sigma m_\nu < 0.13$ eV at 95% CL (in the context of the ΛCDM model) (102).

To reach the 50-meV level with the CMB alone, we need to look at gravitational lensing by intervening structure as the photons travel from the last scattering surface to us. If we could measure the gravitational lensing strength, then we would have a precision measurement of the integrated growth of structure (from the present to the time of last scattering). We have already seen that the neutrinos damp the power spectrum in a scale-dependent manner. Neutrinos cannot cluster on length scales smaller than the free-streaming scale, which affects dark matter perturbations. Thus, on scales smaller than the neutrino free-streaming scale, the matter power spectrum will be suppressed.

The suppression of the amplitude is sensitive to the total energy density of the neutrinos, Ω_ν, as discussed above. Thus, in order to extract the sum of neutrino masses from the CMB or other large-scale structure experiments, we must assume something about the momentum distribution of the neutrinos. If there is a discrepancy between the cosmological and laboratory measurements in the future, it could indicate new physics. If the laboratory constraints require a smaller mass than cosmological measurements in the future, then this could be due to other light degrees of freedom that are contributing to the cosmological measurement. If a laboratory measurement is larger than the cosmological constraint, it could be that new physics makes the neutrino abundance subthermal.

4.2. Number of Light Degrees of Freedom

Neutrinos that are relativistic at the time of last scattering contribute to the relativistic energy density, parameterized as $N_{\rm eff}$. $N_{\rm eff}$ is also, to the consternation of some, called the number of neutrinos. In order to make the connection between $N_{\rm eff}$ and the number of neutrinos, we must assume that the only relativistic particles populating the Universe, other than photons, are neutrinos, and that their abundance is given by the usual thermal prediction. Thus, deviations of $N_{\rm eff}$ from the canonical value of three also signifies new physics.

There is a beautiful and robust way to determine $N_{\rm eff}$ through its effect on the phase shifts in the primary CMB spectrum (39). In the presence of free-streaming particles, the peaks pick up a small shift in phase, which has recently been measured (40). This phase shift is created by only the portion of $N_{\rm eff}$ that is free streaming—that is, noninteracting—and it is very difficult for other cosmological parameters to mimic this signal (103).

In addition, the total $N_{\rm eff}$ (whether free streaming or not) also changes the Silk diffusion damping of the CMB power spectrum. This damping is evident in the CMB power spectrum as the sharp drop in power at $\ell \gtrsim 1{,}000$. The energy density of the relativistic particles contributes to the expansion rate at last scattering, $H_{\rm LSS}$. The peak locations (modulo the phase shifts discussed above) are determined by the sound horizon, which scales as $1/H_{\rm LSS}$, whereas the diffusion damping length scales as $1/H_{\rm LSS}^{1/2}$ because of the stochastic nature of the diffusion process. Thus, the heights of the peaks (determined by the ratio of the two scales) can provide information about the energy density of relativistic particles. Here, one of the main degeneracies is with the helium fraction, which a joint analysis with standard Big Bang nucleosynthesis (BBN) predictions could break (104).

4.3. Consistency of Big Bang Nucleosynthesis and the Cosmic Microwave Background

The CMB enables precision measurements of the baryon density at last scattering, and in the future it will do the same for the helium fraction and N_{eff}. During BBN, these parameters determine the light-element abundances. Thus, in the future it will become possible to perform a precision comparison of BBN and CMB in this three-dimensional plane. Any inconsistencies would imply new physics between the epochs of BBN and last scattering. Future CMB experiments are expected to reduce the error on the helium fraction to 0.005, which is probably better than we can do directly through BBN by using light-element abundances. Including this constraint in BBN calculations will allow us to obtain N_{eff} at an accuracy comparable to what can be achieved from the phase shift of the peaks or the amplitude of Silk diffusion damping.

Lepton number is another parameter in the neutrino sector with very weak constraints. The CMB is sensitive to lepton number through the increase in $N_{\mathrm{eff}} = (30/7\pi^2)\xi^2 + (15/7\pi^4)\xi^4$, where the chemical potential ξ sets the lepton number relative to photons as $\pi^2\xi(1+\xi^2/\pi^2)/[12\zeta(2)]$. The constraints on ξ are of order unity, if we use the current constraints on N_{eff}. In terms of the neutrino chemical potential, the BBN is more sensitive to ξ_e compared with $\xi_{\mu,\tau}$ because the former affects the neutron–proton conversion rate. The current constraint is $\xi_e < 0.2$.

4.4. Lensing of the Cosmic Microwave Background and Neutrino Mass

The suppression described above in the discussion of large-scale structure is also imprinted in the power spectrum of lensing potential. Lensing of the CMB maps the unlensed temperature or polarization ($\tilde{X}$) into the lensed sky X as $X(\mathbf{n}) = \tilde{X}(\mathbf{n} + \delta\mathbf{n})$ (105). The deflections $\delta\mathbf{n}$ in the directions of photons create a distinct non-Gaussian pattern in the CMB, which allows the lensing potential to be measured (106).

These deflections are given by the gradient of the lensing potential ϕ, which is integrated over the path of the photon (in the Born approximation). If we set the curvature of the Universe to zero, this quantity can be written as

$$\phi(\mathbf{n}) = 2\int_0^{r_s} dr\,\Psi(r\mathbf{n}, r)(r - r_s)/(rr_s)\,, \qquad 11.$$

where r is the coordinate distance along our past light cone, r_s is the coordinate distance to the last scattering surface, and $\delta\mathbf{n} = \nabla\phi$. The deflections are typically of order arcminutes. However, these deflections are correlated over degree scales because of the intervening large-scale structure that creates these deflections. This is reflected in the power spectrum of the deflection angle, which peaks around $L \simeq 40$.

Thus, the suppression of the matter power spectrum is directly imprinted in the gravitational potential and, hence, in the deflection angle spectrum. The suppression for $k < k_{\mathrm{fs}}$ is converted to the multipole scale $L \gtrsim k_{\mathrm{fs}} d_{\mathrm{A}}(z)$, where d_{A} is the angular diameter distance and the redshift $z \approx 2$ because the window function, determined by the $(r - r_s)/(rr_s)$ term in Equation 11, attains its maximum around that redshift. Thus, the deflection angle power spectrum should be suppressed for $L \gtrsim 10$ (**Figure 2**).

To measure Σm_ν values as low as 50 meV through CMB lensing, we need to be able to determine the primordial power spectrum to an accuracy better than 1%. The normalization of the

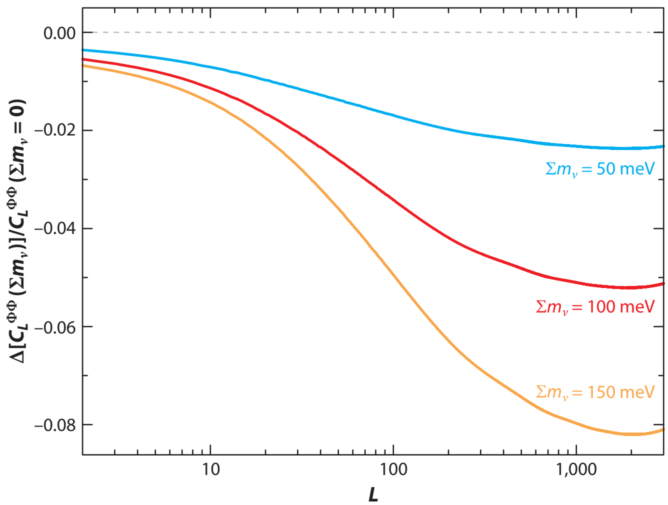

Figure 2

The changes to the power spectrum of the lensing potential (related to the deflection angle due to gravitational lensing) when neutrinos are given masses as indicated. The total matter density today is kept fixed. The changes shown here mirror the scale-dependent suppression in the power spectrum of matter perturbations.

large-ℓ CMB power spectrum (beyond the first peak) is governed by the primordial power spectrum multiplied by $\exp(-2\tau)$, where τ is the optical depth to electron scattering. When this combination is constrained well by the CMB, the uncertainties on τ dominate the error on the primordial power spectrum. The current 1σ error on τ from Planck data is 0.013, and with some more improvement, we expect to be able to reach 50 meV at 1σ with future experiments (28, 107).

The other major degeneracies for the measurement of the neutrino mass are the parameters of evolving dark energy and curvature of the Universe (89, 108, 109). If we parameterize dark energy as a fluid with a constant equation of state w, then the effect of w on C_L^{ϕ} is roughly constant with L and, hence, can be distinguished from the scale-dependent effect of neutrino mass (107). However, if we allow for the presence of dark energy at early times, then the errors become larger, and the addition of other data sets with different degeneracy directions may become important to recover constraints at the 50-meV level.

4.5. Forecasts for Neutrino Mass Measurements

In the near future, data from Planck and from polarized South Pole Telescope (SPT-POL) and Atacama Cosmology Telescope (ACTPol) surveys will yield results for the sum of neutrino masses with a precision of 0.1 eV, when combined with large-scale structure data sets such as that from BOSS. The 0.1-eV scale is key: If $\Sigma m_\nu < 0.1$ eV, then we know that the neutrino masses have the normal ordering (**Figure 3**). There are plans to upgrade SPT-POL to SPT-3G, which will yield a 20-fold increase in mapping speed and, thus, improve the ability to cover a large chunk of the sky. Similarly, there are plans for an Advanced ACTPol that can measure CMB polarization over half the sky. Both experiments, in combination with data sets such as that from BOSS, promise to achieve a sensitivity of Σm_ν close to 0.05 eV (110). Unfortunately, this is still not enough to rule out the inverted hierarchy at 3σ or greater outright, but it may be possible to do so in combination with long-baseline and reactor experiments.

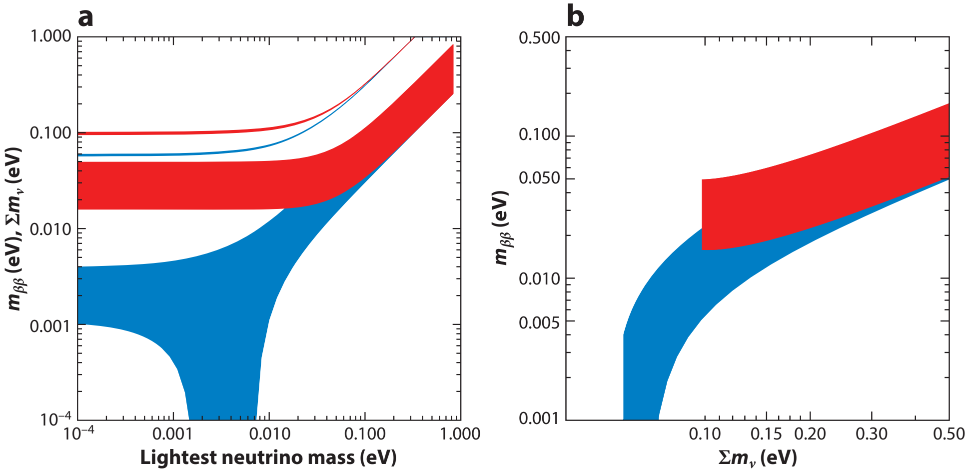

Figure 3

(*a*) The allowed regions for the sum of neutrino masses Σm_ν (*top two curves*) and the neutrino mass that controls the double-β decay rate $m_{\beta\beta}$ (assuming that the zero-neutrino double-β transition is due to the neutrino mass term). The red shaded region assumes inverted ordering, and the blue shaded region assumes normal ordering for the neutrino mass hierarchy. (*b*) The $m_{\beta\beta}$ range plotted against the Σm_ν values, for which we choose the average of the allowed range.

Research following up on the Snowmass Community Summer Study (111) has addressed the possibility of a future Stage-IV CMB polarization experiment (CMB-S4). Including the possibility of future data from DESI, these studies (112) forecast 1σ errors on Σm_ν of 15 meV and on $N_{\rm eff}$ of 0.016. Such results from CMB-S4 would be extraordinary. Not only would this experiment perform a $>3\sigma$ detection of the sum of neutrino masses; it would also test the neutrino decoupling corrections to $N_{\rm eff}$ (the distinction between $N_{\rm eff}$ values of 3 and 3.045). The $N_{\rm eff}$ test will also become a precision probe of other light degrees of freedom, such as those one may expect from dark sectors.

5. CONCLUSIONS

The prospect that the study of the largest structures in the Universe can produce the most sensitive measures of the mass and number neutrinos is very exciting. The standard cosmological model, with a handful of parameters, successfully describes both the history of the observable Universe and the growth of structure in it. The cosmological parameters of this model have been measured to percent-level precision (62).

As described in detail above, the continuation of this successful program in cosmological physics, with no upcoming surprises, is predicted to provide high sensitivity to the neutrino mass hierarchy and to enable measurement of the sum of the neutrino masses. The current experiments have also measured the relativistic energy density to ∼10% accuracy, and future experiments may even be sensitive to the standard enhancement in the neutrino number density from electron–positron annihilation during the BBN epoch.

These predictions depend on the standard cosmological model being accurate, so there are inherent model dependencies in the neutrino mass determination via cosmology. These include a standard thermal history for the Universe, the validity of general relativity at large scales, and the influence of dark energy on the expansion history and the growth of structure. Relaxation of these assumptions can partially relax the sensitivity of cosmological neutrino measures. These model dependencies exist in addition to systematic and nonlinear modeling uncertainties that may be present in any given observational study. Such model dependencies can be tested as the sensitivity of observations increases, making the probes more robust.

The next decade of cosmological observations will provide a wealth of new measurements of cosmological expansion history and the growth of large-scale structure, as well as the primordial perturbation spectrum. Additionally, cosmological observations will contribute to measurements of the fundamental properties of the most elusive standard model particle: the neutrino.

DISCLOSURE STATEMENT

The authors are not aware of any affiliations, memberships, funding, or financial holdings that might be perceived as affecting the objectivity of this review.

ACKNOWLEDGMENTS

K.N.A. was partially supported by NSF CAREER grant PHY-11-59224. K.N.A. and M.K. are partially supported by NSF grant PHY-1316792.

LITERATURE CITED

1. Riess AG, et al. *Astron. J.* 116:1009 (1998)
2. Perlmutter S, et al. *Astrophys. J.* 517:565 (1999)
3. Guth AH. *Phys. Rep.* 333:555 (2000)
4. Fukuda Y, et al. *Phys. Rev. Lett.* 81:1562 (1998)
5. Cleveland BT, et al. *Astrophys. J.* 496:505 (1998)
6. Ahmad QR, et al. *Phys. Rev. Lett.* 89:011301 (2002)
7. Aguilar-Arevalo AA, et al. *Phys. Rev. D* 64:112007 (2001)
8. Aguilar-Arevalo AA, et al. *Phys. Rev. Lett.* 98:231801 (2007)
9. Huber P. *Phys. Rev. C* 84:024617 (2011); Huber P. Erratum. *Phys. Rev. C* 85:029901 (2012)
10. Kopp J, Machado PAN, Maltoni M, Schwetz T. *J. High Energy Phys.* 05:050 (2013)
11. Olive KA, et al. *Chin. Phys. C* 38:090001 (2014)
12. Hu W, Eisenstein DJ, Tegmark M. *Phys. Rev. Lett.* 80:5255 (1998)
13. Gonzalez-Garcia MC, Maltoni M, Schwetz T. arXiv:1512.06856 [hep-ph] (2015)
14. Beck M. *J. Phys. Conf. Ser.* 203:012097 (2010)
15. Avignone FT III, Elliott SR, Engel J. *Rev. Mod. Phys.* 80:481 (2008)
16. Mohapatra RN, Smirnov AY. *Annu. Rev. Nucl. Part. Sci.* 56:569 (2006)
17. Fixsen DJ. *Astrophys. J.* 707:916 (2009)
18. Kolb EW, Turner MS. *The Early Universe.* Redwood City, CA: Addison-Wesley (1990)
19. Lopez RE, Turner MS. *Phys. Rev. D* 59:103502 (1999)
20. Mangano G, et al. *Nucl. Phys. B* 729:221 (2005)
21. Grohs E, et al. arXiv:1512.02205 [astro-ph.CO] (2015)
22. Kawasaki M, Kohri K, Moroi T. *Phys. Rev. D* 63:103502 (2001)
23. Giudice GF, Kolb EW, Riotto A. *Phys. Rev. D* 64:023508 (2001)
24. Langacker P. Report UPR-0401T, SLAC, Stanford, CA (1989)
25. Chacko Z, Hall LJ, Okui T, Oliver SJ. *Phys. Rev. D* 70:085008 (2004)
26. Dodelson S. *Modern Cosmology.* San Diego: Academic (2003)
27. Hu W, Eisenstein DJ. *Astrophys. J.* 498:497 (1998)
28. Lesgourgues J, Pastor S. *Phys. Rep.* 429:307 (2006)
29. Bond JR, Efstathiou G, Silk J. *Phys. Rev. Lett.* 45:1980 (1980)
30. Abazajian KN, Dodelson S. *Phys. Rev. Lett.* 91:041301 (2003)

31. Foot R, Volkas RR. *Phys. Rev. Lett.* 75:4350 (1995)
32. Abazajian K, Bell NF, Fuller GM, Wong YYY. *Phys. Rev. D* 72:063004 (2005)
33. Bell NF, Pierpaoli E, Sigurdson K. *Phys. Rev. D* 73:063523 (2006)
34. Hannestad S, Raffelt G. *Phys. Rev. D* 72:103514 (2005)
35. Chacko Z, Hall LJ, Oliver SJ, Perelstein M. *Phys. Rev. Lett.* 94:111801 (2005)
36. Ghalsasi A, Nelson AE. *Phys. Rev. D* 90:045002 (2014)
37. Hannestad S. *J. Cosmol. Astropart. Phys.* 0502:011 (2005)
38. Cyr-Racine FY, Sigurdson K. *Phys. Rev. D* 90:123533 (2014)
39. Bashinsky S, Seljak U. *Phys. Rev. D* 69:083002 (2004)
40. Follin B, Knox L, Millea M, Pan Z. *Phys. Rev. Lett.* 115:091301 (2015)
41. Smith TL, Das S, Zahn O. *Phys. Rev. D* 85:023001 (2012)
42. Singh S, Ma CP. *Phys. Rev. D* 67:023506 (2003)
43. Ringwald A, Wong YYY. *J. Cosmol. Astropart. Phys.* 0412:005 (2004)
44. Betts S, et al. Presented at Community Summer Study 2013: Snowmass on the Mississippi (CSS2013), Minneapolis, July 29–Aug. 6 (2013)
45. Brandbyge J, Hannestad S, Haugbølle T, Wong YYY. *J. Cosmol. Astropart. Phys.* 1009:014 (2010)
46. Abazajian K, et al. *Phys. Rev. D* 71:043507 (2005)
47. Marulli F, et al. *Mon. Not. R. Astron. Soc.* 418:346 (2011)
48. Villaescusa-Navarro F, et al. *J. Cosmol. Astropart. Phys.* 1403:011 (2014)
49. Scherrer RJ, Weinberg DH. *Astrophys. J.* 504:607 (1998)
50. Elgaroy O, et al. *Phys. Rev. Lett.* 89:061301 (2002)
51. Tegmark M, et al. *Phys. Rev. D* 69:103501 (2004)
52. Tegmark M, et al. *Phys. Rev. D* 74:123507 (2006)
53. Reid BA, et al. *Mon. Not. R. Astron. Soc.* 404:60 (2010)
54. Eisenstein DJ, Hu W, Tegmark M. *Astrophys. J.* 518:2 (1999)
55. Cuesta AJ, Niro V, Verde L. arXiv:1511.05983 [astro-ph.CO] (2015)
56. Bartelmann M, Schneider P. *Phys. Rep.* 340:291 (2001)
57. Cooray AR. *Astron. Astrophys.* 348:31 (1999)
58. Huterer D, Takada M, Bernstein G, Jain B. *Mon. Not. R. Astron. Soc.* 366:101 (2006)
59. Bassett BA, Hlozek R. In *Dark Energy: Observational and Theoretical Approaches*, ed. P Ruiz-Lapuente, p. 246. Cambridge, UK: Cambridge Univ. Press (2010)
60. Dawson KS, et al. *Astron. J.* 145:10 (2013)
61. Eisenstein DJ, Seo HJ, White MJ. *Astrophys. J.* 664:660 (2007)
62. Ade PAR, et al. arXiv:1502.01589 [astro-ph.CO] (2015)
63. Ross AJ, et al. *Mon. Not. R. Astron. Soc.* 449:835 (2015)
64. Anderson L, et al. *Mon. Not. R. Astron. Soc.* 441:24 (2014)
65. Beutler F, et al. *Mon. Not. R. Astron. Soc.* 416:3017 (2011)
66. Cen R, Miralda-Escudé J, Ostriker JP, Rauch M. *Astrophys. J.* 437:L9 (1994)
67. Croft RAC, et al. *Astrophys. J.* 520:1 (1999)
68. Croft RAC, Hu W, Dave R. *Phys. Rev. Lett.* 83:1092 (1999)
69. McDonald P, et al. *Astrophys. J.* 635:761 (2005)
70. Lai K, Lidz A, Hernquist L, Zaldarriaga M. *Astrophys. J.* 644:61 (2006)
71. Peeples MS, et al. *Mon. Not. R. Astron. Soc.* 404:1295 (2010)
72. Wang S, et al. *Phys. Rev. Lett.* 95:011302 (2005)
73. Pierpaoli E, Scott D, White MJ. *Mon. Not. R. Astron. Soc.* 325:77 (2001)
74. Huterer D, White MJ. *Astrophys. J.* 578:L95 (2002)
75. Rossetti M, et al. arXiv:1512.00410 [astro-ph.CO] (2015)
76. Trac H, Gnedin NY. *Adv. Sci. Lett.* 4:228 (2011)
77. Bowman JD, Morales MF, Hewitt JN. (MWA Collab.) *Bull. Am. Astron. Soc.* 43:218 (abstr.) (2001)
78. Ali ZS, et al. *Astrophys. J.* 809:61 (2015)
79. Ghosh A, et al. *Mon. Not. R. Astron. Soc.* 426:3295 (2012)

80. Röttgering HJA, et al. In *Proceedings of the Conference on Cosmology, Galaxy Formation and Astro-Particle Physics on the Pathway to the SKA*, ed. HR Klöckner, S Rawlings, M Jarvis, A Taylor, p. 169. Oxford, UK: Oxford Univ.
81. Mao Y, et al. *Phys. Rev. D* 78:023529 (2008)
82. Pritchard JR, Pierpaoli E. *Phys. Rev. D* 78:065009 (2008)
83. Dawson KS, et al. arXiv:1508.04473 [astro-ph.CO] (2015)
84. Zhao GB, et al. arXiv:1510.08216 [astro-ph.CO] (2015)
85. Flaugher B. *Int. J. Mod. Phys. A* 20:3121 (2005)
86. Font-Ribera A, et al. *J. Cosmol. Astropart. Phys.* 1405:023 (2014)
87. Levi M, et al. arXiv:1308.0847 [astro-ph.CO] (2013)
88. Abate A, et al. arXiv:1211.0310 [astro-ph.CO] (2012)
89. Joudaki S, Kaplinghat M. *Phys. Rev. D* 86:023526 (2012)
90. Basse T, et al. *J. Cosmol. Astropart. Phys.* 1405:021 (2014)
91. Amendola L, et al. *Living Rev. Relativ.* 16:6 (2013)
92. Spergel D, et al. arXiv:1503.03757 [astro-ph.IM] (2015)
93. Wyman M, Rudd DH, Vanderveld RA, Hu W. *Phys. Rev. Lett.* 112:051302 (2014)
94. Battye RA, Moss A. *Phys. Rev. Lett.* 112:051303 (2014)
95. Dvorkin C, Wyman M, Rudd DH, Hu W. *Phys. Rev. D* 90:083503 (2014)
96. Ade PAR, et al. arXiv:1502.01597 [astro-ph.CO] (2015)
97. Abazajian KN. *Astropart. Phys.* 19:303 (2003)
98. Komatsu E, et al. *Astrophys. J. Suppl.* 192:18 (2011)
99. Samtleben D, Staggs S, Winstein B. *Annu. Rev. Nucl. Part. Sci.* 57:245 (2007)
100. de Putter R, et al. *Astrophys. J.* 761:12 (2012)
101. Giusarma E, de Putter R, Ho S, Mena O. *Phys. Rev. D* 88:063515 (2013)
102. Palanque-Delabrouille N, et al. *J. Cosmol. Astropart. Phys.* 1511:011 (2015)
103. Baumann D, Green D, Meyers J, Wallisch B. arXiv:1508.06342 [astro-ph.CO] (2015)
104. Hou Z, et al. *Phys. Rev. D* 87:083008 (2013)
105. Zaldarriaga M, Seljak U. *Phys. Rev. D* 58:023003 (1998)
106. Hu W, Okamoto T. *Astrophys. J.* 574:566 (2002)
107. Kaplinghat M, Knox L, Song YS. *Phys. Rev. Lett.* 91:241301 (2003)
108. Smith KM, Hu W, Kaplinghat M. *Phys. Rev. D* 74:123002 (2006)
109. de Putter R, Zahn O, Linder EV. *Phys. Rev. D* 79:065033 (2009)
110. Benson BA, et al. *Proc. SPIE Int. Soc. Opt. Eng.* 9153:91531P (2014)
111. Feng JL, et al. Presented at Community Summer Study 2013: Snowmass on the Mississippi (CSS2013), Minneapolis, July 29–Aug. 6 (2013)
112. Wu WLK, et al. *Astrophys. J.* 788:138 (2014)